Evidence for very large deformation in neutron deficient nuclei with $Z \simeq 40$

K. Heyde,* J. Moreau, and M. Waroquier
Institute for Nuclear Physics, B-9000 Gent, Belgium
(Received 28 September 1983)

A detailed study of very neutron deficient nuclei with $Z \simeq 40$ (Sr,Zr) and $N \simeq 40$ has been carried out. Total potential energy surfaces taking into account both quadrupole and hexadecapole deformation have been calculated for the Zr ($Z=40$) nuclei, starting from the Nilsson model. Also odd-mass nuclei have subsequently been studied when coupling the odd particle to the deformed even-even core. After extensive band mixing calculations for the $^{79}_{38}Sr_{41}$ nucleus, comparison to the existing experimental data [energy spectra for positive and negative parity $\frac{5}{2}^+[422]$ and $\frac{3}{2}^-[301]$ bands; static moments μ, Q; mixing ratios $\delta(E2/M1)$ and branching ratios] has been carried out. We have also concentrated on the excited state properties of even-even Sr nuclei within the framework of the interacting boson model. A critical analysis of the interacting boson model parameters, as obtained from calculations in nearby nuclei, i.e., $_{34}$Se, $_{36}$Kr, is carried out, especially for the behavior of κ, χ_π, and χ_ν.

NUCLEAR STRUCTURE Total potential energy surface calculations for even-even Zr nuclei ($36 \leq N \leq 60$). Band-mixing calculations for the adjacent odd-mass nucleus ($^{79}_{38}Sr_{41}$). Band-state properties: [μ, Q, $\delta(E2/M1)$, branching ratios]. Excited states in even-even Sr nuclei with $40 \leq N \leq 48$ in the interacting-boson model (IBA-2). Discussion of IBA-2 parameters. Calculation of quadrupole moments $Q(2_1^+)$, nuclear radii and isomer shifts.

I. INTRODUCTION

Strongly deformed nuclei are well known to occur in the rare-earth region ($50 < Z < 82$; $N \gg 82$) and in the actinide region ($82 < Z < 126$; $N \gg 126$). However, it was also shown that, in regions near closed shells, indications for large quadrupole deformation connected with particular intruder orbitals exist.[1] Results, as the outcome of experiments carried out by Lister *et al.*,[2,3] have given clear indications for possibly very large prolate deformation in the neutron deficient $_{38}$Sr nuclei. Quadrupole deformation, deduced from yrast $B(E2)$ values, is consistent with a value of $\epsilon_2 \simeq 0.4$. Similarly, Piercey *et al.*[4] have obtained such experimental evidence for deformed ground states in the very light $_{36}$Kr isotopes.

From the theoretical side, problems do occur when comparing the existing extensive calculations carried out by Möller and Nix,[5] pointing towards large prolate quadrupole deformation with estimates made by Åberg[6] and Bucurescu,[7] indicating a nearly spherical shape in the ground state for such neutron deficient $Z \simeq 40$ nuclei.

In order to get more detailed insight into the sensitivity of such total potential energy (TPE) surface calculations for the $Z \simeq 40$ mass region, we have carried out a detailed and systematic study of the even-even $_{40}$Zr nuclei ($36 \leq N \leq 60$), using the modified Nilsson harmonic oscillator model,[8] including both quadrupole and hexadecapole deformation (see Sec. II A). In Sec. II B, we have extended the present study to include odd-mass nuclei: We carry out a detailed comparison of the $^{79}_{38}Sr_{41}$ experimental data[2] with results of extensive band-mixing calculations, including for the negative parity all $N=3$ levels and all $N=4$ orbitals when considering positive parity levels. Here, we also concentrate on static moments (dipole and quadrupole moments, μ and Q), branching ratios as well as $\delta(E2/M1)$ mixing ratios. In Sec. III, we concentrate on the excited state properties of the even-even $_{38}$Sr nuclei with neutron number $40 \leq N \leq 48$. In light of the results of Sec. II A on TPE surfaces, we expect a smooth change from strongly deformed nuclei ($N \simeq 40$) towards anharmonic vibrational-like spectra (near $N \cong 50$) with single-particle aspects also showing up when approaching the closed neutron $N=50$ shell. These calculations have been carried out in the framework of the interacting boson model, treating proton (π) and neutron (ν) excitations explicitly (IBA-2). We give much attention to a systematic study of IBA-2 parameters ϵ, κ, χ_π, and χ_ν when combining our results concerning the $_{38}$Sr nuclei with existing calculations on Se ($Z=34$) and Kr ($Z=36$) nuclei (see Sec. III for references). Finally, we also briefly discuss the results on electric quadrupole moments for the even-even $_{38}$Sr nuclei as well as isomer and isotope shifts.

II. STUDY OF DEFORMATION PROPERTIES NEAR $Z \simeq 40$

A. Even-even $_{40}$Zr nuclei

Extensive calculations of nuclear masses and deformation (quadrupole, hexadecapole) have been carried out recently[5–7,9] throughout the whole nuclear mass region. All

approaches obtain the total energy of the nucleus as a sum of a macroscopic "liquid drop" term and a microscopic contribution (shell and pairing corrections). The particular way to obtain and combine both contributions has been outlined by Strutinsky.[10] The extensive calculations of Möller and Nix[5] start from a Yukawa-plus-exponential macroscopic model and a folded Yukawa form for the microscopic model calculations, whereas Åberg[6] uses the Nilsson model with quadrupole and triaxial shape coordinates (ϵ_2,γ). Both calculations generally agree but, for particular mass regions, contradicting results are obtained. For the $_{38}$Sr,$_{40}$Zr neutron deficient nuclei (near $N\simeq 40$), Möller and Nix obtain large prolate quadrupole deformed shapes whereas Åberg obtains almost spherical shapes. Before elaborating on our Nilsson model calculations, including both quadrupole (ϵ_2) and hexadecapole deformation (ϵ_4), we first give in Fig. 1 a contour plot of the results of Möller and Nix concerning ground state quadrupole moments, defined as,

$$Q_2=2\left[\frac{3Z}{4\pi r_0^3 A}\right]\int r^2 P_2(\cos\theta)d\tau\ , \tag{2.1}$$

with $r_0=1.16$ fm. The contour lines are obtained from the tables of Ref. 5, using an interpolation program. The distance between adjacent contour lines is 0.5 e b; the black region corresponding to values of $Q_2\geq 3.0$ e b. Figure 1 clearly illustrates that near $Z\simeq 40, N\simeq 40$, very large quadrupole deformed ground states can occur, but also that when both Z and N increase, a very rapid variation towards oblate shapes results.

We have carried out, using the modified Nilsson harmonic oscillator model, detailed calculations in order to study the TPE surfaces and also the single-particle and one-quasiparticle (1qp) spectra when keeping $Z=40$, but changing the neutron number in a large interval $(36\leq N\leq 60)$. The liquid drop macroscopic part of the energy is expressed by the mass formula of Seeger and Howard[11] in calculating the liquid drop model energy from the same parametrization of the nuclear surface as used in the calculation of the Nilsson single-particle spectra. For the single-particle spectra, we use values as interpolated between the light nuclei $(A\simeq 40)$ and the strongly deformed rare-earth nuclei,[12,13] e.g., $\kappa_\pi=0.069$, $\mu_\pi=0.475$; $\kappa_\nu=0.07$, $\mu_\nu=0.323$ (for $^{80}_{40}$Zr$_{40}$), and use as pairing strength,

$$G=19.2A+7.4(N-Z)/A^2\ , \tag{2.2}$$

with the + and − sign for protons and neutrons, respectively, with $\sqrt{10Z}$ or $\sqrt{10N}$ levels above and below the Fermi level taken into account when calculating the pairing energy correction. This particular prescription, moreover, reproduces well the experimental odd-even mass differences for the mass region we concentrate on in the present study.

In Fig. 2, we indicate part of the Nilsson single-particle spectrum as calculated for the $^{80}_{40}$Zr$_{40}$ nucleus, calculated as a function of the quadrupole deformation ϵ_2. On the horizontal axis however, we indicate (ϵ_2,ϵ_4) since actually, as in some of the following figures, we calculate the Nilsson single-particle energies along the minimum total potential energy curve in the (ϵ_2,ϵ_4) plane. This means that for each ϵ_2 value, we have calculated properties for the corresponding ϵ_4 value related to the minimum in the total potential energy surface in the hexadecapole direction. Thereby, the only good quantum numbers that remain are the Ω^π quantum numbers as indicated on the single-particle orbitals. We also explicitly include the $N\rightarrow N+2$ mixing matrix elements that show up when otherwise Nilsson orbitals Ω^π with $\Delta N=2$ would be crossing at a particular value of the deformation coordinates. In this particular single particle spectrum, one already clearly observes that for ϵ_2 values around $\epsilon_2\cong 0.4$, the proton and/or neutron number 38 will form a well stabilized deformed shell and thus, for nuclei where $Z\simeq 40$ $(38\leq Z\leq 42)$, the $N=38$ configuration will probably form a strongly quadrupole deformed nucleus. This is in sharp contrast with the observation of a spherical subshell closure around N (or $Z)\simeq 40$ when Z (or N) is close to or equal to the configuration with 28 or 50 protons (or neutrons), respectively. The deformation driving tendency for particular single-particle orbitals at or near $N=38$ for the Zr nuclei is most clearly exhibited when presenting the behavior of Nilsson one-quasiparticle (1qp) energies (see Fig. 3),

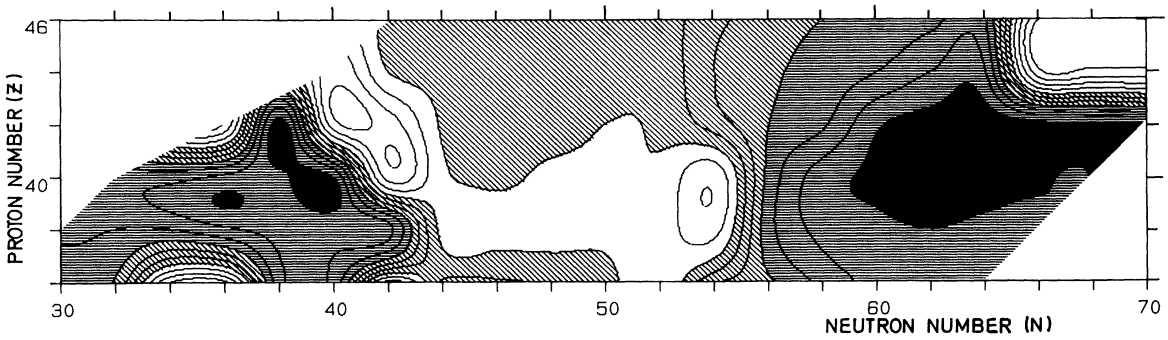

FIG. 1. Contour map, indicating the ground state quadrupole moments, defined in Eq. (2.1) for the region $36\leq Z\leq 46, 30\leq N\leq 70$. The distance between adjacent contour lines is $\Delta E=0.5$ e b, and the black region corresponds to a value $Q_2\geq 3$ e b.

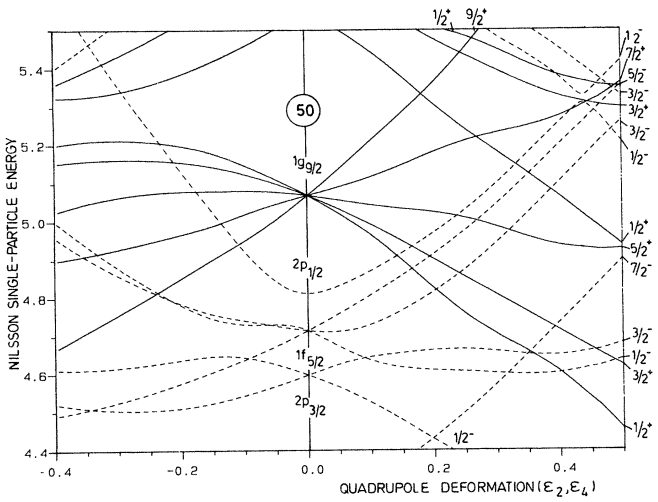

FIG. 2. Part of the Nilsson single-particle level scheme for the nucleus $^{80}_{40}Zr_{40}$ as a function of the quadrupole deformation ϵ_2. On the horizontal axis, we, however, indicate (ϵ_2,ϵ_4) since in many other figures we have calculated along a line, minimizing the total potential energy surface (TPE) in the hexadecapole deformation ϵ_4. The single-particle levels are identified via the remaining good quantum numbers Ω^π.

$$E(\Omega^\pi)=\sqrt{[\epsilon(\Omega^\pi)-\lambda]^2+\Delta^2}\ . \tag{2.3}$$

In this particular figure, the 1qp states originating from the $1g_{9/2}$, $2p_{1/2}$, $2p_{3/2}$, and $1f_{5/2}$ orbitals are presented with increasing neutron number ($N=38$, $N=42$, $N=46$). Especially for the $N=38$ nucleus, one observes an energy gain of $\simeq 1.5$ MeV when a nucleus becomes deformed (near $\epsilon_2\simeq 0.4$) with respect to the spherical 1qp energy. This tendency completely disappears when the neutron number increases towards the neutron shell closure at $N=50$. Here, the $2p_{1/2}$ orbital has a very strong deformation dependent 1qp energy in the interval $0.0\le\epsilon_2\le 0.4$. If now (as clearly shown in Fig. 5), the total potential energy of the even-even nucleus is rather flat in the quadrupole deformation interval $-0.4\le\epsilon_2\le 0.5$, the particular deformation of 1qp energies will be the major driving mechanism in establishing strongly deformed bands in odd-mass nuclei (see Sec. II B for application to the nucleus $^{79}_{38}Sr_{41}$), especially when the neutron number is very near the $N\simeq 40$ configuration.

The detailed results for the TPE surfaces in the even-even Zr nuclei, with neutron number $36\le N\le 60$, have been calculated and some typical results are shown in Fig. 4, where contour lines indicate the detailed topology in the quadrupole (ϵ_2)-hexadecapole (ϵ_4) plane. The distance between adjacent contour lines is $\Delta E=0.5$ MeV. One can pictorially see the prolate minimum (for $N>38$) move away and also observe that the soft oblate minima coalesce in forming a single minimum, moving towards sphericity when N increases towards $N=50$. Beyond $N=50$, a very pronounced oblate and prolate minimum develops, the latter being the deepest one. If we now make a cut along the minimum of the TPE surface in the (ϵ_2,ϵ_4) plane [indicated with a dashed line in Figs. 4(a) and (b)], we obtain Fig. 5, where a still more clear-cut overview of TPE surface changes with increasing neutron number N is

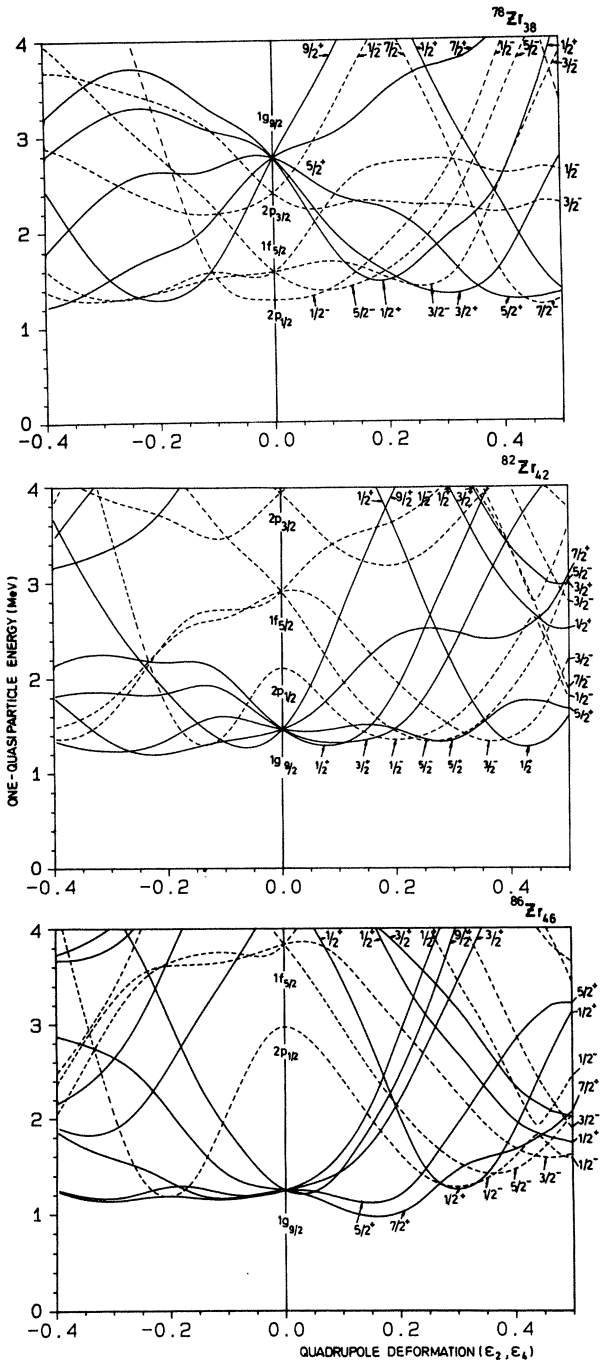

FIG. 3. Nilsson one-quasiparticle energies E_{1qp} [see Eq. (2.3)] for the nuclei $^{78}_{40}Zr_{38}$, $^{82}_{40}Zr_{42}$, and $^{86}_{40}Zr_{46}$, as a function of the quadrupole deformation, including minimization along the TPE in the hexadecapole deformation, i.e., (ϵ_2,ϵ_4). The full lines denote positive parity orbitals whereas the dashed lines originate from negative parity orbitals. The quantum numbers are denoted on the single-particle levels as Ω^π.

presented. Here, it is very clear that in the region of neutron number $36\le N\le 40$, the TPE surfaces do not exhibit a very pronounced prolate or oblate minimum. One can thus estimate that small changes in the parameters of the Nilsson model (κ,μ) when adding an odd proton or neu-

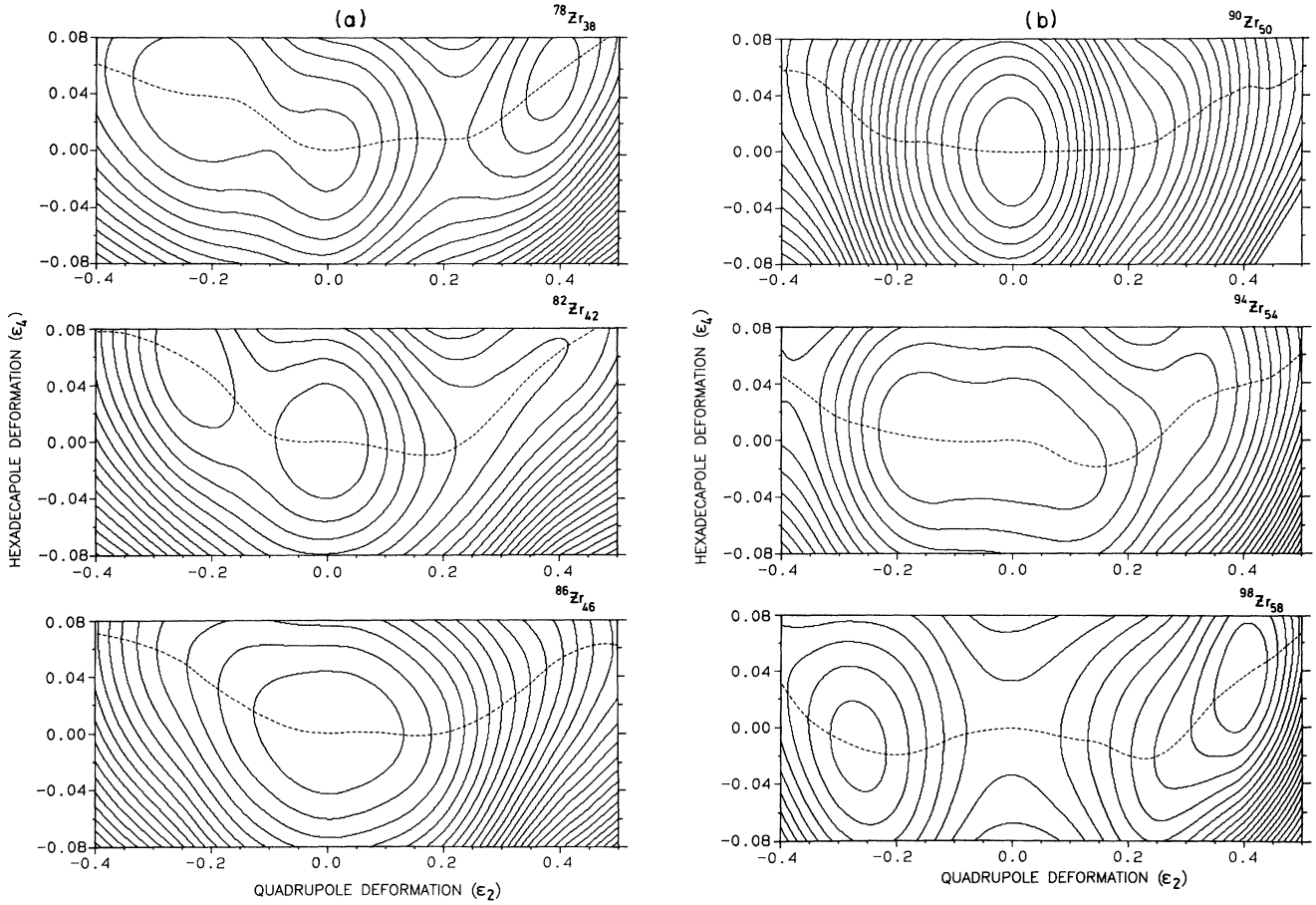

FIG. 4. (a) The total potential energy surface (TPE) for the ^{78,82,86}Zr even-even nuclei, as a function of the quadrupole (ϵ_2) and hexadecapole (ϵ_4) deformation. Contour lines are spaced at an interval of $\Delta E = 0.5$ MeV. The minimum in the TPE is drawn as the dashed line, and has been used to calculate single particle (Fig. 2) energies and 1qp (Fig. 3) energies. (b) Same as (a) but for ^{90,94,98}Zr.

tron in discussing the adjacent odd-mass nuclei, will influence the TPE surfaces in a decisive way. Thus, one conclusion of the systematic and detailed study carried out here is that the calculations of Möller and Nix[5] and Åberg[6] can in no way be a unique calculation of fixing the ground state mass of the nucleus and its deformation characteristics. Whenever one is obtaining a prolate, oblate, or spherical shape as lowest minimum in the ground state of the Zr nuclei with neutron number $36 \leq N \leq 40$, the particular minimum will be dependent on the choice of the Nilsson model parameters κ,μ determining both the macroscopic properties (liquid drop energy behavior) and the microscopic shell and pairing corrections. This latter statement is dramatically illustrated in the $^{80}_{40}Zr_{40}$ nucleus (see Fig. 6) where for a varying μ_ν parameter, the TPE has been calculated. Particular cuts along the lines *A*, *B*, and *C* (see Fig. 6) make this contour surface more easily transparent for inspection.

As a particular conclusion of this subsection, we can state that contrary to the unique predictions of Refs. 5–7, a critical examination of the TPE surface incorporating both quadrupole and hexadecapole deformation in a modified harmonic oscillator Nilsson model is able to shed light on the particular dependence of the obtained large prolate and oblate deformation in the neutron deficient nuclei with $Z \simeq 40$ and $N \simeq 40$. Although TPE surfaces are obtained that are very soft against quadrupole deformation with both minima in the prolate and oblate shape configuration, no unique choice can be made from the present calculations. In the adjacent odd-mass nuclei, the odd particle will polarize the even-even core nucleus into a well defined oblate or prolate shape dependent on the particular Nilsson orbital. We shall concentrate on this topic in the next subsection. Finally, we mention that although the detailed calculations were carried out for the even-even Zr nuclei, results for the $_{38}$Sr and $_{42}$Mo nuclei will be very similar.

B. Band-mixing calculations for $^{79}_{38}Sr_{41}$

Since very detailed experimental data exist on the neutron deficient $^{79}_{38}Sr_{41}$ nucleus,[2,3] we have carried out, guided by the TPE surface calculations for adjacent even-even nuclei, extensive band-mixing calculations for both positive and negative parity levels in the $^{79}_{38}Sr_{41}$ nucleus; the main configurations containing the odd-neutron moving in the $\frac{5}{2}^+[422]$ or $\frac{3}{2}^-[301]$ Nilsson orbitals, respectively. Only treating these pure orbitals however, is too restrictive to obtain a good description of the observed band structure. Following the detailed discussions as outlined in

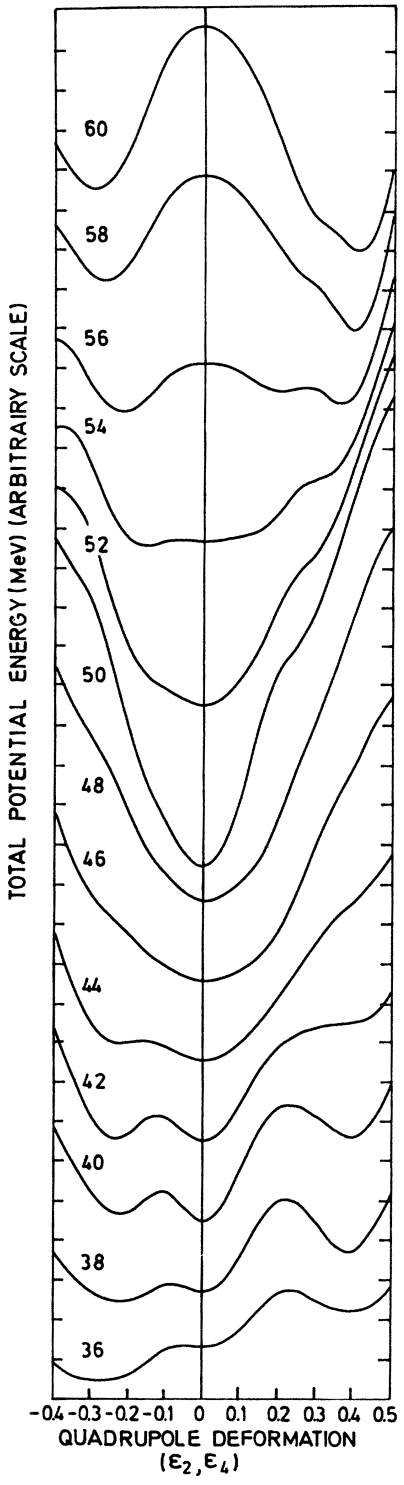

FIG. 5. The total potential energy for the even-even Zr nuclei with neutron number $36 \leq N \leq 60$, along the dashed line of Figs. 4(a) and (b). Thus, the horizontal axis gives the combined deformation (ϵ_2, ϵ_4).

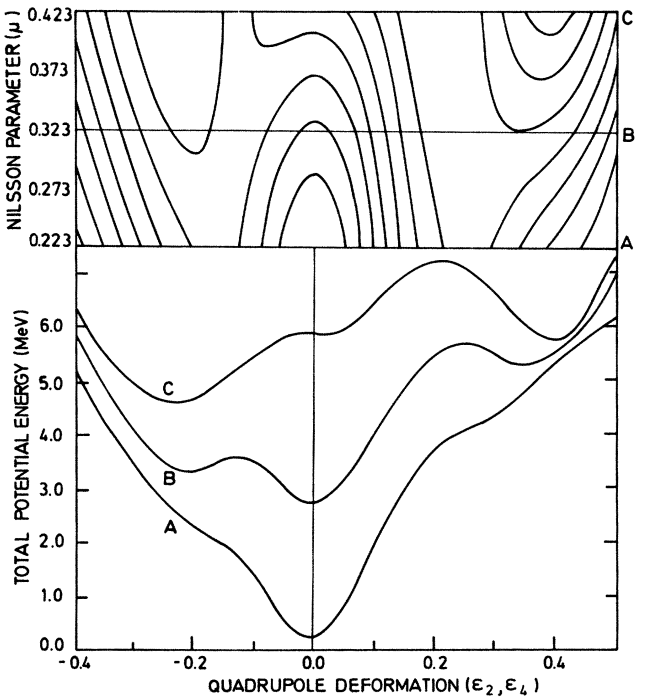

FIG. 6. Variation of the total potential energy surface for the nucleus ^{80}Zr, when varying the Nilsson model parameter μ_ν in the interval $0.223 \leq \mu_\nu \leq 0.423$ along the line of minimal potential energy, calculated for $\mu_\nu = 0.323$. Three different cuts, along the lines denoted *A*, *B*, and *C*, are shown in the lower part of the figure, in their detailed total potential energy dependence on (ϵ_2, ϵ_4) deformation parameters.

Refs. 1 and 14–20, all Nilsson orbitals in the $N=3$ oscillator shell (for negative parity levels) and in the $N=4$ oscillator shell (for positive parity) are considered in a band-mixing calculation.

Starting from a deformed basis and using the strong-coupling wave functions[21] $|(\Omega,i)JM\rangle$, one can diagonalize the Hamiltonian describing the even-even core and the odd particle coupled to the rotational motion of the even-even core,

$$H = H_{\text{core}} + H_{\text{sp}} , \tag{2.4}$$

with

$$H_{\text{core}} = \frac{\hbar^2}{2\mathcal{J}} \vec{R}^2 , \tag{2.5}$$

and

$$H_{\text{sp}} = \sum_{\Omega,i} E(\Omega,i) a^\dagger_{\Omega,i} a_{\Omega,i} , \tag{2.6}$$

where $\vec{R}$ describes the core angular momentum and $E(\Omega,i)$ the 1qp energies obtained from the Nilsson model when including pairing correlations (see Sec. II A). The nuclear matrix elements then become

$$\langle(\Omega',i')JM \mid H \mid (\Omega,i)JM\rangle = 2\sum_{j,J_c} (-1)^{j-\Omega}\langle j\Omega, j-\Omega \mid J_c 0\rangle (-1)^{j-\Omega'}\langle j\Omega', j-\Omega' \mid J_c 0\rangle E_{J_c} c_j(\Omega,i) c_j(\Omega',i')$$
$$\times (u_{\Omega,i}u_{\Omega',i'} + v_{\Omega,i}v_{\Omega',i'}) + E(\Omega,i)\delta_{\Omega\Omega'}\delta_{ii'} . \tag{2.7}$$

Here, E_{J_c} denotes the core excitation energies [eigenvalues corresponding with the collective Hamiltonian of Eq. (2.5)] and are taken from the $^{78}_{38}Sr_{40}$ experimental level scheme[2] for the yrast band. The Nilsson wave functions, denoted by the expansion coefficients $c_j(\Omega,i)$, occupation probabilities $v^2_{\Omega,i}$, as well as $E(\Omega,i)$ (1qp energies), have been calculated in the interval $-0.4 \leq \epsilon_2 \leq 0.5$ (see Sec. II A). If we now intend to describe states with $J^\pi \leq \frac{21}{2}^-$ and $\leq \frac{19}{2}^+$, core yrast states up to $J^\pi_c = 14^+$ must be considered and have been taken from Ref. 2. The final wave functions then become

$$|J^\alpha M\rangle = \sum_{\Omega,i} d^\alpha(\Omega,i;J)\,|(\Omega,i)JM\rangle\ , \tag{2.8}$$

when expressed in the strong-coupling basis. Transforming to a weak-coupling basis with fixed core- and single-particle (sp) angular momentum,[17] one gets

$$|J^\alpha M\rangle = \sum_{j,J_c} \{U_{j,J_c}(J^\alpha)[c^\dagger_{j,m}\,|\,J_c M_c\rangle]_{JM} + V_{j,J_c}(J^\alpha)[\tilde{c}_{j,m}\,|\,J_c M_c\rangle]_{JM}\}\ , \tag{2.9}$$

with

$$U_{j,J_c}(J^\alpha) \equiv \sum_{\Omega,i} [2(2J_c+1)/(2J+1)]^{1/2}\langle j\Omega J_c 0\,|\,J\Omega\rangle c_j(\Omega,i) d^\alpha(\Omega,i;J) u_{\Omega,i}\ , \tag{2.10}$$

and similarly for $V_{j,J_c}(J^\alpha)$.

Besides calculating energy levels, we have also calculated the static moments (μ,Q), $B(E2;\Delta J=2)$, $B(E2;\Delta J=1)$ as well as $B(M1;\Delta J=1)$ transition matrix elements. The expressions are not given here but we refer to Refs. 17–19 for a detailed discussion of the corresponding operators and reduced transition matrix elements. Here now, however, we shall concentrate on a comparison of the calculated results with the experimental data of Lister *et al.*[2,3]

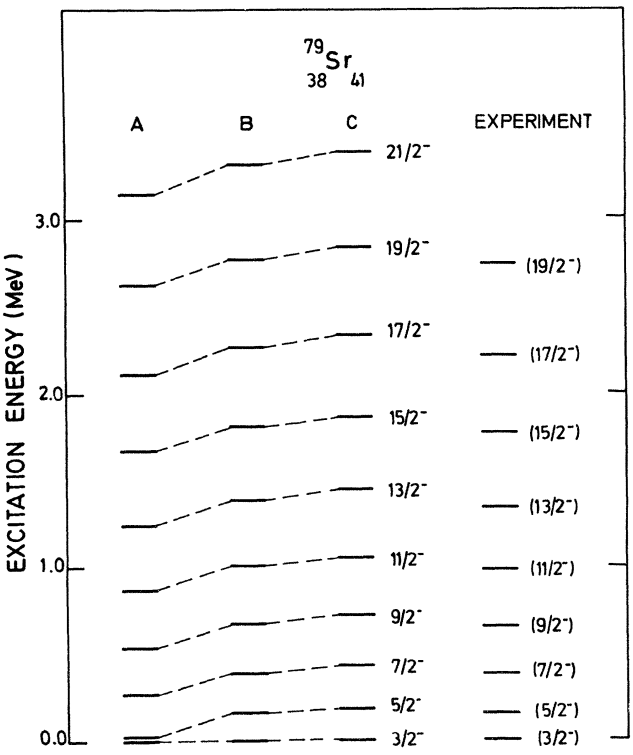

FIG. 7. Negative parity band, built on the $\frac{3}{2}^-[301]$ orbital in $^{79}_{38}Sr_{41}$, as a function of the quadrupole deformation. The results *A*, *B*, and *C* correspond to $\epsilon_2=0.30$, $\epsilon_2=0.35$, and $\epsilon_2=0.40$, respectively. The resulting band is obtained after a full $N=3$ band mixing calculation [Eqs. (2.7) and (2.8)]. The experimental data from the work of Lister *et al.* (Ref. 2) are also given.

In Fig. 7, the negative parity ground state band, starting from the $\frac{3}{2}^-$ band head, being mainly the $\frac{3}{2}^-[301]$ Nilsson orbital, is shown for varying quadrupole deformation ($0.30 \leq \epsilon_2 \leq 0.40$) and compared with the experimental band on the right-hand side of the figure. It can be seen that indeed near neutron number $N=40,42$, the $\frac{3}{2}^-[301]$ and $\frac{5}{2}^+[422]$ orbitals are obtained near the Fermi level and will therefore determine the band structure in the odd-mass $^{79}_{38}Sr_{41}$ nucleus (see also Fig. 3). Very good agreement with the theoretical band-mixing calculation at a value of $\epsilon_2=0.35$ is obtained. The $\frac{3}{2}^-$ level indeed is mainly $\frac{3}{2}^-[301]$ (amplitude of 0.998). For the $\frac{5}{2}^-$ level, the composition [see Eq. (2.8)] becomes

$$|\tfrac{5}{2}^-_1\rangle \cong 0.94\,|[301];\tfrac{5}{2}^-\rangle + 0.34\,|[303],\tfrac{5}{2}^-\rangle\ , \tag{2.11}$$

showing the importance of the band mixing clearly.

All other electromagnetic properties have been calculated using the particular value of $\epsilon_2=0.35$ for the quadrupole deformation. In Fig. 8, the magnetic dipole moment and the intrinsic quadrupole moment have been calculated. In calculating the dipole moment we have used the value of $g_l=0$, $g_s=0.7g_s^{\text{free}}$, and $g_R=Z/A$ and a value of $B(E2;0^+_1\rightarrow 2^+_1)=1.1\ e^2b^2$ for the calculation of $E2$ properties. The latter value corresponds with the experimental half-life of 155 ± 19 psec of the 2^+_1 level in $^{78}_{38}Sr_{40}$.[2] The intrinsic quadrupole moment was subsequently obtained from the laboratory value, using the relation

$$Q_{\text{intr}} = \frac{(I+1)(2I+3)}{3\Omega^2 - I(I+1)} Q_{\text{lab}}\ . \tag{2.12}$$

The full lines indicate results obtained for the pure $\frac{3}{2}^-[301]$ band whereas the dashed line gives the analogous results for a full $N=3$ shell band-mixing calculation [see Eq. (2.8)]. The large drop at $J^\pi=\frac{5}{2}^-$ for Q_{intr} is owing to extracting the intrinsic quadrupole moment from the band-mixing calculation where in between the value of J ($\frac{3}{2} < J < \frac{5}{2}$), the sign of the denominator changes and small changes in the Q_{lab} value influence the determination of the intrinsic quadrupole moment in an important way. This result is probably unphysical and by small ad-

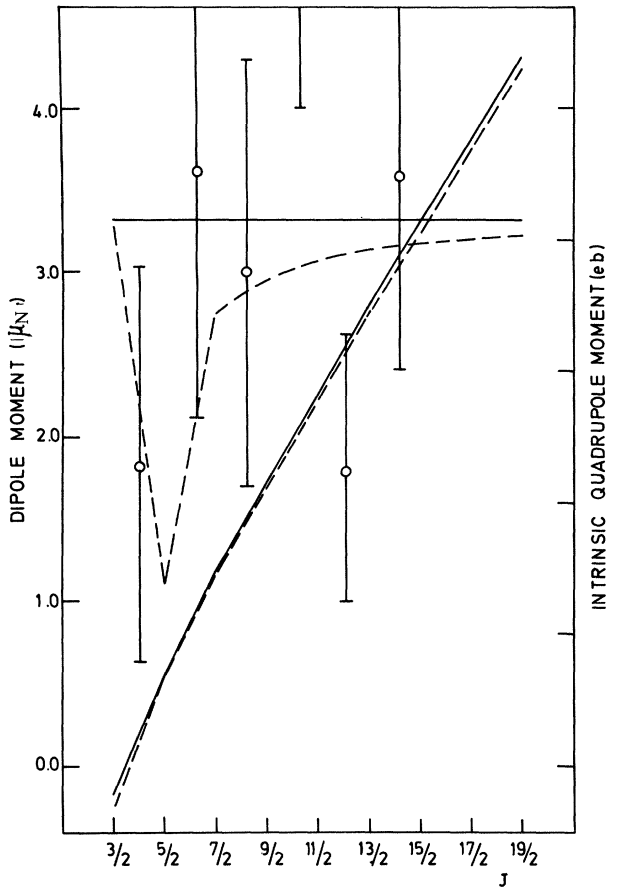

FIG. 8. Static quadrupole moments [converted into the intrinsic quadrupole moment, Eq. (2.12) (e b)] and magnetic dipole moments for the $\frac{3}{2}^-$ band in $^{79}_{38}Sr_{41}$. The smooth up sloping line indicates the dipole moments. Experimental, intrinsic quadrupole moments (right-hand scale) with error bars (Ref. 2) are also given. The full lines refer to the pure $\frac{3}{2}^-[301]$ band whereas the dashed lines are the result of a full band mixing calculation.

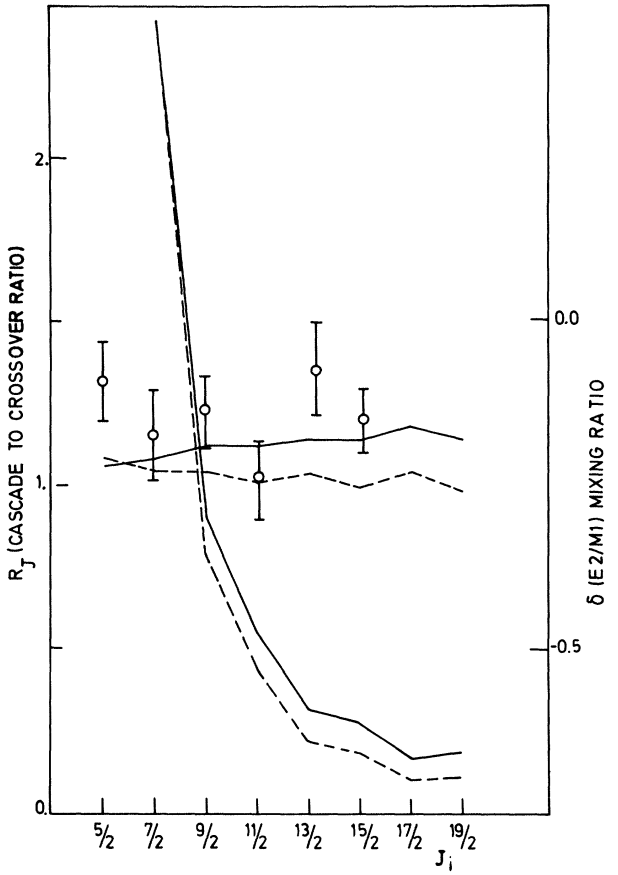

FIG. 9. Cascade mixing ratios $\delta(E2/M1)$ (right-hand scale) and cascade-to-crossover ratio R_J. The initial angular momentum is given as J_i. Again, the convention of the pure $\frac{3}{2}^-[301]$ band and full $N=3$ band mixing applies for the full and dashed lines, respectively. The experimental data points concerning $\delta(E2/M1)$ are taken from Ref. 2 and compared with the theoretical, almost constant, behavior.

mixtures in the $J^\pi=\frac{5}{2}^-$ wave function, other then the $\frac{3}{2}^-[301]$ orbital [see (2.11)], this particular value of Q_{intr} ($\frac{5}{2}^-$) can easily be affected in an important way. In this same Fig. 8, we also compare experimental values, which are, however, deduced from the reduced $B(E2;\Delta J=1)$ values[2] and thus do not completely compare with the Q_{intr} values as obtained from Eq. (2.12).

In Fig. 9, the cascade ($\Delta J=1$) to crossover ($\Delta J=2$) ratio,

$$\frac{P(E2;\Delta J=1)+P(M1;\Delta J=1)}{P(E2;\Delta J=2)}\ , \tag{2.13}$$

where P denotes the total transition probability (sec^{-1}) and using the experimental gamma deexcitation energies, has been compared to the experimental data of Ref. 2. We have, moreover, used the same effective charge and gyromagnetic factors as outlined before. Here again the full lines denote the calculations using a pure $\frac{3}{2}^-[301]$ band whereas the dashed line results when using the full band-mixing wave functions of Eq. (2.8). Also, the $\delta(E2/M1)$ mixing ratios are presented (right-hand scale) and compared to the experimental data of Ref. 2. Although the general behavior of δ is well described, a fine structure staggering in the experimental data shows up that is not reproduced from the calculations although band mixing slightly improves the agreement. Moreover, the consistent negative sign for the quantity $\delta(E2/M1)$ corroborates the realization of a prolate deformed shape in the particular $\frac{3}{2}^-$ band.

Finally, an interesting quantity can be obtained from the $\Delta J=1$, $M1$ and $E2$ reduced matrix elements, i.e.,

$$\frac{\langle J-1||M1||J\rangle}{\langle J-1||E2||J\rangle}=2\left[\frac{(I+1)(I-1)}{5}\right]^{1/2}\left[\frac{e\hbar}{2mc}\right]\frac{(g_\Omega-g_R)}{Q_{\text{intr}}}[1+\delta_{\Omega,1/2}(-1)^{J+1/2}b_0]\ , \tag{2.14}$$

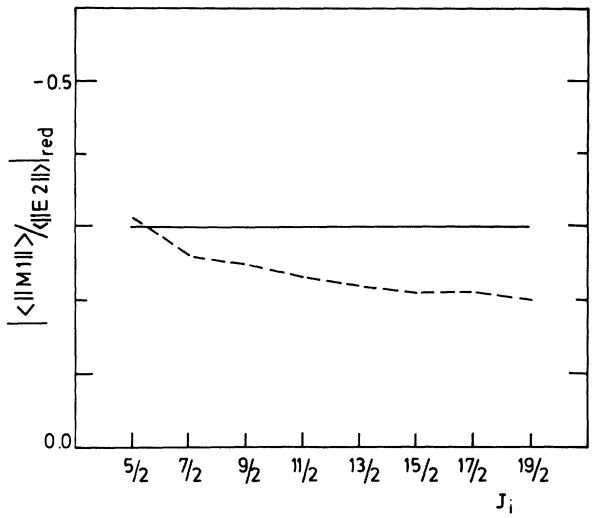

FIG. 10. The reduced $|\langle||M1||\rangle/\langle||E2||\rangle|_{red}$ matrix element, defined in Eq. (2.15), for again pure $\frac{3}{2}^-[301]$ band and band mixing (full and dashed lines, respectively). The initial state angular momentum for this ratio is given as J_i.

and thus the "reduced" $M1/E2$ ratio, defined as

$$\frac{\langle J-1||M1||J\rangle}{\langle J-1||E2||J\rangle}\Big/2\left[\frac{(I+1)(I-1)}{5}\right]^{1/2}, \qquad (2.15)$$

gives the ratio

$$\frac{g_\Omega - g_R}{Q_{\text{intr}}}\left[\frac{\mu_N}{e\,\text{b}}\right],$$

along the $\frac{3}{2}^-$ yrast band. These particular quantities, defined by Eq. (2.15), are shown in Fig. 10 for the pure $\frac{3}{2}^-[301]$ band and including band mixing. For the pure band, the ratio indicates a value of

$$\frac{g_\Omega - g_R}{Q_{\text{intr}}} = -0.30\ (\mu_N/e\,\text{b}),$$

which leads, taking out the intrinsic pure band quadrupole moment, to a value of $g_\Omega - g_R = -1.01$ (-1.30 as an experimental value,[2] using the same gyromagnetic factors).

We also have studied the positive parity band $\frac{5}{2}^+[422]$ and its band structure. We show in Fig. 11 the particular positive parity band as well as its position with respect to the $\frac{3}{2}^-$ ground state band in $^{79}_{38}Sr_{41}$. Here, moreover, we compare the existing experimental data of Ref. 2.

We can indeed conclude that the odd-neutron particle polarizes the underlying even-even core such as to induce stable, large quadrupole deformation with $\epsilon_2 \simeq 0.35$ in order to reproduce the observed spectra. All known data on the negative parity band can be well described using a full $N=3$ oscillator shell band-mixing calculation at $\epsilon_2 = 0.35$.

III. COLLECTIVE EXCITATIONS IN EVEN-EVEN Sr NUCLEI

Although in some nuclei with a proton number near $Z=40$ [the Se nuclei ($Z=34$) (Refs. 22–25) and the Kr nuclei ($Z=36$) (Refs. 26–30)] IBA-2 calculations have been carried out in a systematic way in order to study the low-lying collective excitations, for the Sr nuclei no such systematic and detailed calculations exist (Refs. 31–33). Moreover, we compare the IBA-2 parameters that give a best fit for the Se and Kr nuclei with the present calculations and study these results also in the light of the microscopic estimates of these IBA-2 parameters.[34–36]

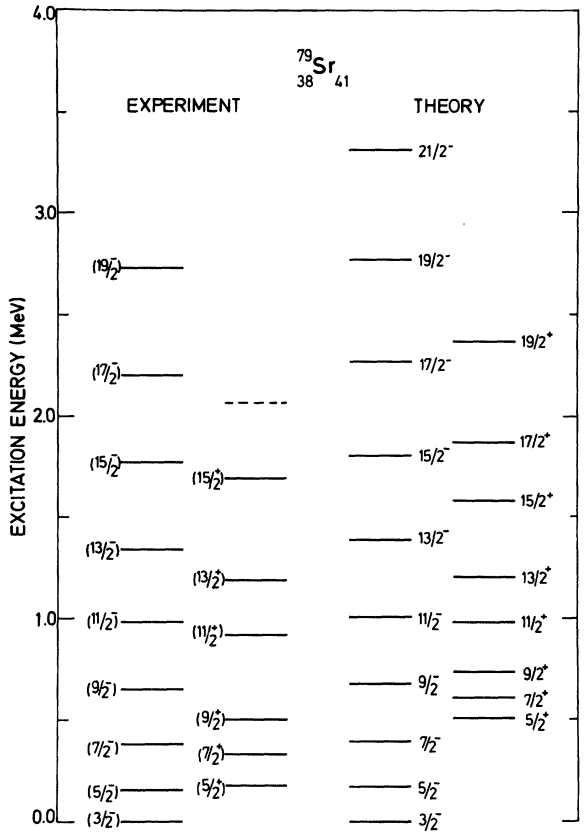

FIG. 11. The comparison of the $^{79}_{38}Sr_{41}$ theoretical and experimental (Ref. 2) level schemes with respect to both the negative and positive parity bands.

The particular features that are causing problems in order to obtain a coherent description of the low-lying collective states ($E_x \lesssim 2.5$ MeV) stem from the fact that in the Se and Kr nuclei with small neutron number, a very low lying 0^+ excited state has been observed.[22,26] The precise origin of this level can be attributed to proton or neutron subshell closure effects. A possible explanation of the particular behavior and its appearance has been suggested by Duval *et al.*[25] in promoting a proton two particle configuration across the $Z=40$ proton subshell closure. This mechanism is, moreover, clearly related to the fact (shown in Sec. II A) that in the nearby Kr nuclei,[4] coexisting shapes—spherical and strongly quadrupole deformed—are observed as close-lying levels in the light $^{74,76}_{36}Kr_{38,40}$ nuclei. The TPE surface calculations for the Zr nuclei (Sec. II A) also point out that, for a neutron number near $N \simeq 40$ ($36 \lesssim N \lesssim 42$), a rather complex TPE surface results, but that from $N > 42$ on, more simple quadrupole excitations will determine the spectra at low

energy. In the Sr nuclei ($Z=38$), the experimental spectra[31–33] show a change from deformed, rotational-like spectra ($0^+,2^+,4^+,6^+,8^+,\ldots,$) near $N\simeq 40$, evolving towards triaxial or γ-soft vibrational spectra when the neutron number N is approaching the closed shell at $N=50$ ($0^+,2^+,2^+,4^+,\ldots,$ sequence). Therefore, we study here, within the framework of IBA-2, the $^{78}_{38}Sr_{40}$-$^{86}_{38}Sr_{48}$ even-even nuclei.

A. IBA-2 parameters

The IBA-2 Hamiltonian, with standard form[37,38] has been used here as

$$H=\epsilon(n_{d_\pi}+n_{d_\nu})+\kappa Q_\pi Q_\nu+M_{\pi\nu}\ , \tag{3.1}$$

where the quadrupole operator is given as

$$Q^{(2)}_{\pi(\nu)}=(d^\dagger s+s^\dagger\tilde{d})^{(2)}_{\pi(\nu)}+\chi_{\pi(\nu)}(d^\dagger\tilde{d})^{(2)}_{\pi(\nu)}\ . \tag{3.2}$$

The boson number operator for protons and neutrons is given by $n_{d_{\pi(\nu)}}$, respectively, and $M_{\pi\nu}$ denotes the Majorana operator (see Refs. 37 and 38).

In Figs. 12–15, the parameters ϵ, κ, χ_ν, and χ_π, respectively, are shown as obtained from a best fit to the low-lying part of the Sr spectra and are given at the same time with the IBA-2 parameters as obtained for the Se and Kr nuclei as obtained by the Köln group in the same mass region.[22,26] In Figs. 14(a) and (b), and 15(a) and (b), we also indicate the microscopic behavior of the κ, χ_ν, and χ_π parameters, respectively.[34–36] It becomes clear that ϵ has the almost constant behavior as expected from the microscopic underlying picture. Only when approaching the $N=50$ neutron shell closure does ϵ (for the Sr nuclei) increase by $\pm 50\%$ with respect to the average ϵ value taken over all other Se, Kr, and Sr nuclei. Moreover, the ϵ values for the three different isotope chains do form a coherent set of single-boson energies.

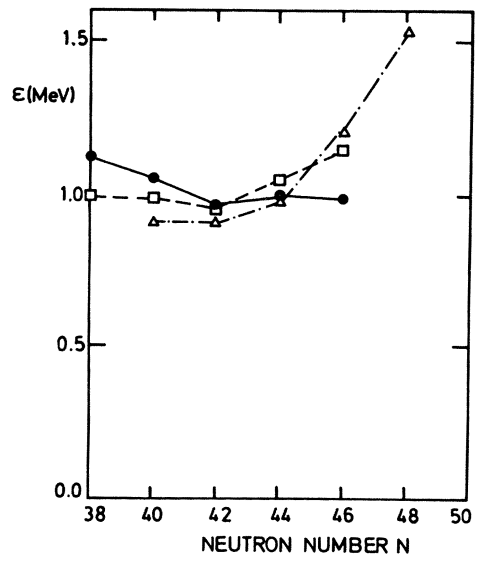

FIG. 12. Graphical representation of the IBA-2 parameter ϵ for the Se nuclei (Ref. 22) (filled circles), the Kr nuclei (Ref. 26) (open squares), and Sr nuclei (this work, open triangles) as a function of neutron number $38\leq N\leq 48$.

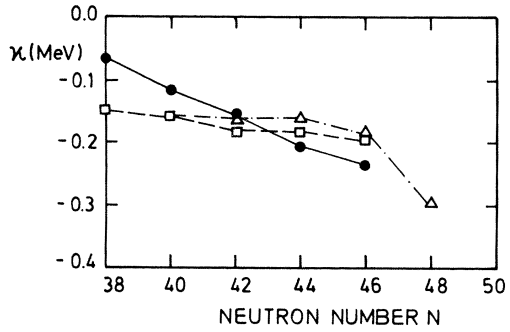

FIG. 13. Same as for Fig. 12, but for the parameter κ.

In inspecting the value of κ (Fig. 13) and comparing it with the possible microscopic estimates [Figs. 14(a) and (b)], again the particular dependence shows up. In the theoretical κ dependence of Fig. 14(a), the upper part considers *all* orbitals in the 28–50 configuration space to form a degenerate orbital with $j_\pi=\frac{21}{2}$, whereas in the lower part, at $Z=40$, a proton subshell closure is considered thus inducing a different neutron number dependence for κ, as given by[37]

$$\kappa=\kappa_0[(\Omega_\nu-N_\nu)(\Omega_\pi-N_\pi)]^{1/2}\ , \tag{3.3}$$

where $\Omega_{\pi(\nu)}$ describes the single-particle degeneracy, i.e.,

$$2\Omega_{\pi(\nu)}=2j_{\pi(\nu)}+1\ , \tag{3.4}$$

and $N_{\pi(\nu)}$ is defined as

$$\begin{aligned} &N=N' \text{ if } 2N'\leq\Omega\ , \\ &N=\Omega-N' \text{ if } 2N'\geq\Omega\ , \end{aligned} \tag{3.5}$$

where $2N'$ describes the number of fermions occupying the single-particle orbital j, i.e., considering $(j)^{2N'}$ configurations. It is difficult to extract out of Fig. 13, in comparing it with the theoretical behavior of κ in Fig. 14(a), evidence for a subshell closure at $Z=40$. However, the

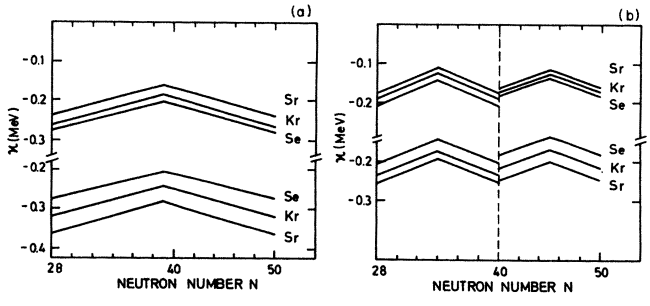

FIG. 14. The theoretical κ dependence, as indicated in Eqs. (3.3)–(3.5), for Se, Kr, and Sr nuclei. On the *left-hand side,* we take the full 28-50 neutron shell a single $j_\nu=\frac{21}{2}$ shell, whereas on the *right-hand side* we consider an $N=40$ subshell closure. In the *upper part* of both figures, we also take the full 28-50 proton shell to be a single $j_\pi=\frac{21}{2}$ shell whereas in the *lower part* we consider a $Z=40$ proton subshell closure.

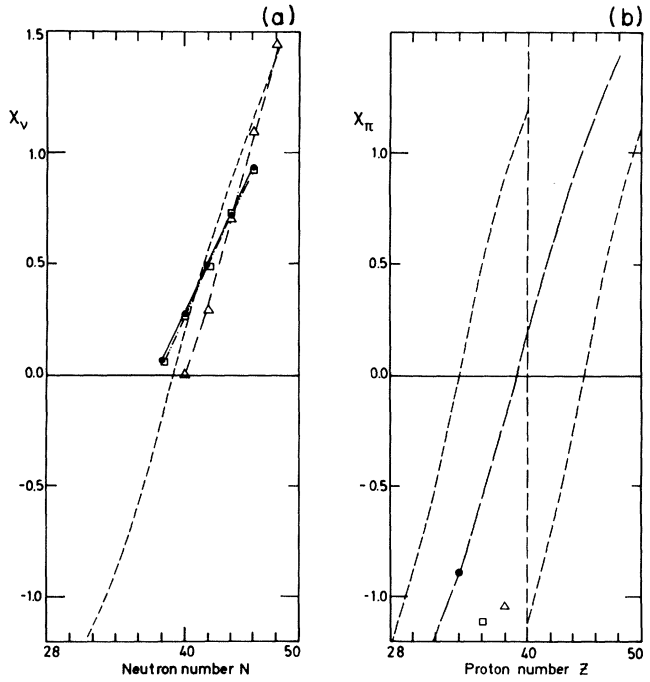

FIG. 15. (a) Same caption as for Fig. 12, but for the IBA-2 parameter χ_ν. Here also (see the dashed line), the microscopic, single $j_\nu=\frac{21}{2}$ level estimate is drawn according to Eq. (3.6). (b) Same as for Fig. 12, but for the IBA-2 parameter χ_π. Here also (see the long dashed line), the microscopic, single $j_\pi=\frac{21}{2}$ level estimate (Eq. 3.6) is drawn. Moreover, when considering a $Z=40$ proton subshell closure, the estimate of Eq. (3.6) changes in an important way, as indicated by the small dashed line.

values of κ near $N=38,40$ are in better agreement with the lower part (having a subshell closure at $Z=40$), whereas at the end of the neutron open shell, near $N\simeq 50$, it seems as if the upper part of Fig. 14(a) is better reproduced. This correlation, however, is only weak. In Fig. 14(b), the dependence of κ, given in Eq. (3.3) but now also including a subshell closure at neutron number $N=40$, is given. The upper part [as in Fig. 14(a)] replaces all valence shells in between 28 and 50 by a degenerate $j_\pi=\frac{21}{2}$ orbital whereas in the lower part, a subshell closure at $Z=40$ is implied.

The χ_ν dependence is given in Fig. 15(a), where a very pronounced correlation with the microscopic estimate,

$$\chi_{\pi(\nu)}=\chi_{0,\pi(\nu)}\frac{\Omega_{\pi(\nu)}-2N'_{\pi(\nu)}}{(\Omega_{\pi(\nu)}-N_{\pi(\nu)})^{1/2}}\ , \tag{3.6}$$

(dashed line) shows up. The value of χ_π, on the other hand [Fig. 15(b)], shows the same microscopic estimate of Eq. (3.6), but also illustrates the χ_π dependence when at $Z=40$ a proton subshell closure is present (small dashed line). The parameters, determined from fits to the Se, Kr, and Sr nuclei are in extreme contrast with one degenerate $j_\pi=\frac{21}{2}$ shell but also the microscopic estimate for two subshells $j_\pi=\frac{11}{2}$ and $\frac{9}{2}$ does not show a good correspondence. Duval and Barrett, however,[35,36] have shown that for a sequence of two shells, the microscopic behavior at the crossing point is smooth and the fitted χ_π parameters do correlate rather well with the calculated χ behavior. Thereby additional evidence for a proton subshell at $Z=40$ results for the considered mass region.

B. IBA-2 calculations for even-even Sr nuclei

With the parameters discussed above and using as the Majorana parameters, the same values as used for the Pd, Ru region,[39] the theoretical and experimental energy spectra are compared in Fig. 16. Here, one immediately observes, from inspecting the theoretical calculations, a smooth change of SU(3)-type spectra near $N\simeq 40$ towards 0(6)-type spectra for N, approximating $N\simeq 50$. These calculated spectra also show that near $Z\simeq 40$ and $N\simeq 40$, strongly deformed nuclei are present and thus, the results obtained here are in line with results obtained in Secs. II A and II B. The transition for the higher-lying $J_i^\pi=2_2^+,4_1^+$ levels with an increasing neutron number is well in agreement with the experimental data.

The quadrupole moments for the $J_i^\pi=2_1^+$ level have also been calculated in some detail, using as an effective charge the arbitrary scale $e=e_\pi=e_\nu=0.1$ e b, and making use of the quadrupole $E2$ operator, given in Eq. (3.2).

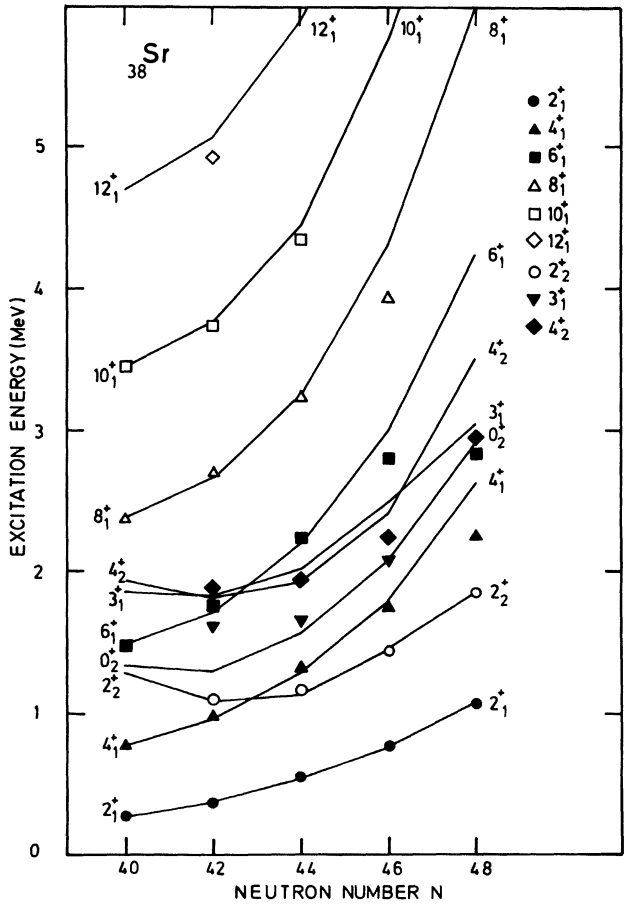

FIG. 16. The calculated IBA-2 spectra for the even-even Sr nuclei with neutron number $40\leq N\leq 48$ for the levels as indicated (full lines). The experimental data are indicated on the same figure, the legend of which is given in detail on the figure itself. The data result from Refs. 2, 3, and 31–33.

In Fig. 17, we decompose $Q(2_1^+)$ in the proton and neutron component. For $N \simeq 40$, large negative values result whereas near the closed shell $N \simeq 50$ region, the signs of both components have changed, leading towards small positive values of the laboratory quadrupole moments. It is interesting to see that the neutron and proton $Q(2_1^+)$ components show a very similar behavior as a function of the neutron number. Since no quadrupole moments are known as yet in this region of nuclei, the values for $Q(2_1^+)$ shown in Fig. 17 are only relative and are given in arbitrary units. The value of the effective charge $e = 0.1\ e$ b that has been used is already most reasonable as seen when comparing it with other IBA-2 calculations, carried out for the even-even Ru and Pd nuclei ($e \sim 0.106\ e$ b).[39]

Finally, we briefly discuss the results from $E0$ moment calculations in giving information on isotope and isomer shifts. Most of the expressions are discussed in detail by Iachello.[40]

The isotopic shift $\Delta\langle r^2\rangle$ is defined as

$$\Delta\langle r_\pi^2\rangle \equiv \langle r_\pi^2\rangle_{0_1^+}(N_\pi, N_\nu+1) - \langle r_\pi^2\rangle_{0_1^+}(N_\pi, N_\nu) , \quad (3.7)$$

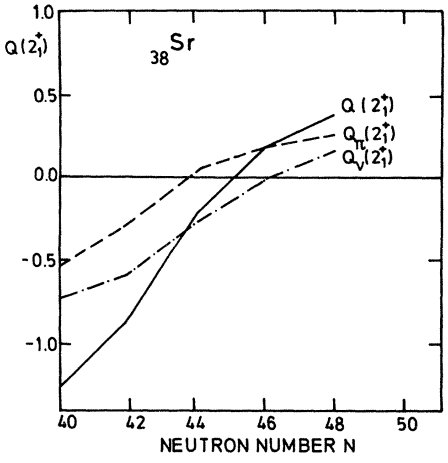

FIG. 17. The calculated IBA-2 quadrupole moments $Q(2_1^+)$ for the even-even Sr nuclei (full line), as well as the separate proton and neutron contributions (dashed and dashed-dotted lines, respectively), using an arbitrary scale (using $e_\pi = e_\nu = e = 0.1\ e$ b).

or rewritten in detail as the following:

$$\Delta\langle r_\pi^2\rangle = \gamma_{\pi\nu}^{(0)} + \beta_{\pi\pi}^{(0)}[\langle n_{d_\pi}\rangle_{0_1^+}(N_\pi, N_\nu+1) - \langle n_{d_\pi}\rangle_{0_1^+}(N_\pi, N_\nu)] + \beta_{\pi\nu}^{(0)}[\langle n_{d_\nu}\rangle_{0_1^+}(N_\pi, N_\nu+1) - \langle n_{d_\nu}\rangle_{0_1^+}(N_\pi, N_\nu)] , \quad (3.8)$$

whereas the isomer shift is denoted by

$$\delta\langle r_\pi^2\rangle \equiv \langle r_\pi^2\rangle_{2_1^+}(N_\pi, N_\nu) - \langle r_\pi^2\rangle_{0_1^+}(N_\pi, N_\nu) , \quad (3.9)$$

or rewritten in detail as the following:

$$\delta\langle r_\pi^2\rangle = \beta_{\pi\pi}^{(0)}[\langle n_{d_\pi}\rangle_{2_1^+}(N_\pi, N_\nu) - \langle n_{d_\pi}\rangle_{0_1^+}(N_\pi, N_\nu)] + \beta_{\pi\nu}^{(0)}[\langle n_{d_\nu}\rangle_{2_1^+}(N_\pi, N_\nu) - \langle n_{d_\nu}\rangle_{0_1^+}(N_\pi, N_\nu)] . \quad (3.10)$$

The quantities $\beta_{\pi\pi}^{(0)}$, $\beta_{\pi\nu}^{(0)}$, and $\gamma_{\pi\nu}^{(0)}$ are considered as parameters in the IBA-2 calculations and fitted via known isotopic and isomer shifts. The expectation values of the d-boson number operator have to be calculated in the ground state and 2_1^+ levels. Furthermore, we indicate with N_π and N_ν the proton and neutron boson number, counting from $Z = 50$ and $N = 50$ as a reference core.

The isotopic shift is able to give information on the change in the mean-square proton radii when approaching the $Z = 40$ and $N \simeq 40$ region. These results are presented in Fig. 18, where we only take into account the proton-dependent part of Eq. (3.8) (putting $\gamma_{\pi\nu}^{(0)} = 0$ as a reference level and taking also $\beta_{\pi\nu}^{(0)} = 0$, as in Ref. 40). Here, we use again an arbitrary scale; however, we use the value $\beta_{\pi\pi}^{(0)} = 0.10$ fm^2.[40] A clear-cut jump in the proton radius results in passing from 44 neutrons to 42 neutrons which indicates that one starts approaching the region of large quadrupole deformation. This result is corroborated by the total potential energy surface calculations (see Sec. II A) combined with the expression for the isotopic shift

$$\Delta\langle r^2\rangle = \tfrac{4}{5} R_0^2 A^{-1/3} + \frac{3}{4\pi} R_0^2 A^{2/3} \Delta\langle \beta^2\rangle , \quad (3.11)$$

when considering axially deformed nuclei for which the

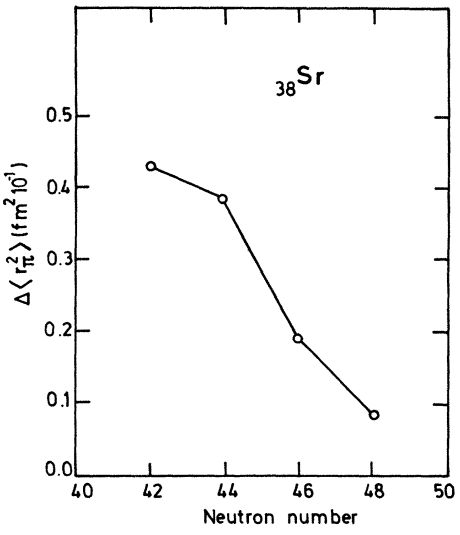

FIG. 18. Isotopic shifts for the even-even Sr nuclei $\Delta\langle r_\pi^2\rangle$, defined in Eqs. (3.7) and (3.8) as a function of neutron number. In the present calculation, we have taken arbitrary units, although from the analysis of Ref. 40 we use $\beta_{\pi\nu}^{(0)} = 0$ and $\beta_{\pi\pi}^{(0)} = 0.1$ fm^2 as realistic estimates of the parameters.

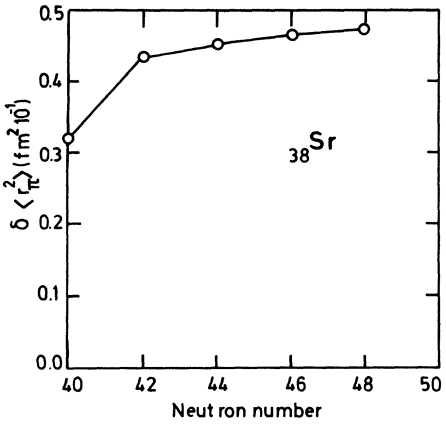

FIG. 19. Using the same parameter values used in Fig. 18, we display the isomer shifts for the even-even Sr nuclei, as a function of the neutron number [see Eqs. (3.9) and (3.10)].

density distribution is characterized by a collective deformation variable β.

The isomer shift, using the same values of $\beta_{\pi\pi}^{(0)}$ and $\beta_{\pi\nu}^{(0)}$, is shown in Fig. 19, in arbitrary units, as a function of a neutron number. For both the isotopic and isomer shift calculations, detailed experimental efforts would be interesting in order to shed light on the possible onset of large quadrupole deformation near $N=40$, evolving into a well defined spherical shape near the closed shell $N=50$ configuration.

IV. CONCLUSION

Besides strongly deformed nuclei in the rare-earth region and in the actinide region, other regions, even near closed shell configurations, have been observed recently. Coexisting levels with largely different shapes at almost the same excitation energy have been measured near $Z\cong 40$ (Se, Kr, Sr, and Zr) when the neutron number approaches the $N\simeq 40$ region. Total potential energy surface calculations show softness against quadrupole deformation with competition between prolate and oblate minima in the even-even Zr nuclei with $N\simeq 40$ where detailed calculations have been carried out. In coupling an odd-particle to the even-even core nuclei, band structure in odd-mass nuclei ($^{79}_{38}Sr_{41}$) could be described in detail. Extensive band mixing calculations were performed and electromagnetic band properties were also studied in detail.

The excited, low lying collective states in even-even nuclei in this particular mass region $Z\simeq 40$ ($40\leq N\leq 48$) have been studied in the framework of the interacting boson model (IBA-2). Detailed parameter studies have been carried out for the Se, Kr, and Sr nuclei and indications for a proton subshell closure at $Z=40$ emerge. This subshell closure is in agreement with the observation of low-lying excited 0^+ states in nuclei with a proton number near $Z\simeq 40$. Energy spectra have been calculated for the Sr nuclei ($Z=38,40\leq N\leq 48$). Good results and agreement with experiment are obtained and the changing level structure from deformed rotor (near $N\simeq 40$) to γ-soft vibrational ($N\simeq 50$) is well described. We finally discussed the quadrupole moment for the 2_1^+ level and concentrated on isotope and isomer shifts for the even-even Sr nuclei. The isotope shifts again point towards an important increase in the proton mean-square radius in going from $N=44$ to 42, in agreement with the calculations carried out in the first part of this study.

An article by D. Bucurescu *et al.*[41] on neutron deficient Sr and Zr has recently appeared. They concentrate on IBA-1 studies (making *no* distinction between protons and neutrons) of the same nuclei and they also perform IBFA calculations. Thereby, their study has no detailed connection with the proton and neutron degrees of freedom that are basic to a detailed understanding of the phenomena occurring in these neutron deficient Sr,Zr nuclei.

ACKNOWLEDGMENTS

The authors are most grateful to F. Iachello for discussions. They are also indebted to the Interuniversitair Institut voor Kernwetenschappen (IIKW) for financial support. Moreover M.W. and J.M. acknowledge the National Fonds voor Wetenschappelijk Onderzoek (NFWO) for constant support. This work was partly supported by the North Atlantic Treaty Organization (NATO) (Research Grant RG0565/82).

*Also at: Rijksuniversiteit Gent, STVS&LEKF, Krijgslaan 271,S9-B9000 Gent, Belgium.

[1]K. Heyde, P. Van Isacker, M. Waroquier, J. Wood, and R. A. Meyer, Phys. Rep. (to be published).

[2]C. J. Lister, B. J. Varley, H. G. Price, and J. W. Olness, Phys. Rev. Lett. 49, 308 (1982).

[3]C. J. Lister, B. J. Varley, A. J. Irving, H. G. Price, and J. W. Olness, in Proceedings of the Conference on High Angular Momentum Properties of Nuclei, Oak Ridge, Tennessee, 1982.

[4]R. B. Piercey *et al.*, Phys. Rev. Lett. 47, 1514 (1981).

[5]P. Möller and J. R. Nix, At. Data Nucl. Data Tables 26, 165 (1981).

[6]S. Åberg, Phys. Scr. 25, 23 (1982).

[7]D. Bucurescu *et al.*, Rev. Roum. Phys. 24, 971 (1979).

[8]S. G. Nilsson, C. F. Tsang, A. Sobiczewski, Z. Szymanski, S. Wycech, C. Gustafson, I. L. Lamm, P. Möller, and B. Nilsson, Nucl. Phys. A131, 1 (1969).

[9]I. Ragnarsson, S. G. Nilsson, and R. K. Sheline, Phys. Rep. 45, 1 (1978).

[10]M. Brack, J. Damgaard, A. S. Jensen, H. C. Pauli, V. M. Strutinsky, and C. Y. Wong, Rev. Mod. Phys. 44, 320 (1972).

[11]P. A. Seeger and W. M. Howard, Nucl. Phys. A238, 491 (1975).

[12]I. Ragnarsson, in Proceedings of the International Conference on Properties of Nuclei Far from the Region of β Stability, Leysin, 1970, CERN Report No. 1970-30, 1970, p. 847.

[13]S. E. Larsson, G. Leander, I. Ragnarsson, and N. G. Alenius, Nucl. Phys. A261, 77 (1976).

[14]N. De Takacsy and S. Das Gupta, Nucl. Phys. A263, 237 (1976).

[15]N. De Takacsy and S. Das Gupta, Phys. Rev. C 13, 399 (1976).
[16]S. Das Gupta and N. De Takacsy, Am. J. Phys. 44, 47 (1976).
[17]P. Van Isacker, Ph.D thesis, University of Gent, 1979 (unpublished).
[18]K. Heyde, M. Waroquier, P. Van Isacker, and H. Vincx, Nucl. Phys. A292, 237 (1977).
[19]P. Van Isacker, M. Waroquier, H. Vincx, and K. Heyde, Nucl. Phys. A292, 125 (1977).
[20]M. Huyse, K. Cornelis, G. Lhersonneau, J. Verplancke, W. B. Walters, K. Heyde, P. Van Isacker, M. Waroquier, G. Wenes, and H. Vincx, Nucl. Phys. A352, 247 (1981).
[21]A. Bohr and B. Mottelson, *Nuclear Structure* (Benjamin, New York, 1975), Vol. II.
[22]U. Kaup, C. Mönkmeyer, and P. von Brentano, Z. Phys. A 310, 129 (1983).
[23]T. Matsuzaki and H. Taketani, Nucl. Phys. A390, 413 (1982).
[24]G. Rotbard, M. Vergnes, J. Vernotte, G. Berrier-Ronsin, J. Kalifa, and R. Tamisier, Nucl. Phys. A401, 41 (1983).
[25]J. P. Delaroche, M. Girod, and P. Duval, in *Proceedings of the International Conference on Nuclear Structure,* edited by A. Van Der Woude and B. J. Verhaar (North-Holland, Amsterdam, 1982), Vol. I, p. 200.
[26]U. Kaup and A. Gelberg, Z. Phys. A 293, 311 (1979).
[27]A. Gelberg and U. Kaup, *Interacting Bosons in Nuclear Physics,* edited by F. Iachello (Plenum, New York, 1979), p. 59.
[28]H. P. Hellmeister, U. Kaup, J. Keinonen, K. P. Lieb, R. Rascher, R. Ballini, J. Delaunay, and H. Dumont, Phys. Lett. 85B, 34 (1979).
[29]H. P. Hellmeister, J. Keinonen, K. P. Lieb, U. Kaup, R. Rascher, R. Ballini, J. Delaunay, and H. Dumont, Nucl. Phys. A332, 241 (1979).
[30]R. A. Meyer, J. F. Wild, K. Eskola, M. E. Leino, S. Väisälä, K. Forssten, U. Kaup, and A. Gelberg, Phys. Rev. C 27, 2217 (1983).
[31]T. Higo, S. Matsuki, and T. Yanabu, Nucl. Phys. A343, 224 (1983).
[32]A. Dewald, U. Kaup, W. Gast, A. Gelberg, H. W. Schuh, K. O. Zell, and P. von Brentano, Phys. Rev. C 25, 226 (1982).
[33]A. Dewald, U. Kaup, W. Gast, A. Gelberg, K. O. Zell, and P. von Brentano, in *Proceedings of the Fourth International Conference on Nuclei Far from Stability, Helsingør, 1981,* edited by P. G. Hansen and G. B. Nielson, CERN Report No. 1981-09, 1981, p. 418.
[34]T. Otsuka, A. Arima, and F. Iachello, Nucl. Phys. A309, 1 (1978).
[35]P. D. Duval and B. R. Barrett, Phys. Rev. Lett. 46, 1504 (1981).
[36]P. D. Duval and B. R. Barrett, Phys. Rev. C 24, 1272 (1981).
[37]O. Scholten, Ph.D. thesis, University of Groningen, 1980 (unpublished).
[38]A. Arima and F. Iachello, Annu. Rev. Nucl. Sci. 31, 75 (1981).
[39]P. Van Isacker and G. Puddu, Nucl. Phys. A348, 125 (1980).
[40]F. Iachello, Nucl. Phys. A358, 89C (1980).
[41]D. Bucurescu *et al.*, Nucl. Phys. A401, 22 (1983).